Sensing of Halocarbons Using Femtosecond Laser-Induced Fluorescence

ARTICLE *in* ANALYTICAL CHEMISTRY · SEPTEMBER 2004

Impact Factor: 5.64 · DOI: 10.1021/ac049425k · Source: PubMed

5 AUTHORS, INCLUDING:

Denis Boudreau
Laval University
49 PUBLICATIONS **1,436** CITATIONS

SEE PROFILE

Anal. Chem. **2004,** *76,* 4799−4805

Sensing of Halocarbons Using Femtosecond Laser-Induced Fluorescence

J.-F. Gravel,[‡] Q. Luo,[‡] D. Boudreau,*[,†] X. P. Tang,[‡] and S. L. Chin[‡]

Department of Chemistry and Centre d'Optique, Photonique et Laser (COPL), and Department of Physics, Physical Engineering and Optics and Centre d'Optique, Photonique et Laser (COPL), Université Laval, Québec (QC), Canada G1K 7P4

A femtosecond laser-induced clean fluorescence technique was explored as a means to monitor halogenated alkanes in the atmosphere. Characteristic difluorocarbene radical (CF_2) fluorescence in the UV−vis can be generated inside a femtosecond laser-induced filament for different halocarbons. We show that, due to different dissociation and excitation kinetics leading to fluorescence emission, it is possible to temporally resolve the characteristic fluorescence of CF_2-containing halocarbons from that of background species, therefore enhancing the signal-to-noise ratio. Laboratory-scale experiments demonstrate the potential use of femtosecond laser-induced clean fluorescence for the remote sensing of halocarbons in the atmosphere. The combination of this detection strategy with LIDAR could allow the long-range monitoring of several atmospheric species with a single laser source, eventually leading to a better understanding of chemical and dynamic processes affecting global warming, ozone loss, tropospheric pollution, and weather prediction.

The key role of atmospheric trace species on many environmental issues such as global warming, stratospheric ozone depletion, and photochemical smog formation is now well recognized, and the knowledge of the fate and behavior of pollutants in the troposphere, as well as the ability to measure their concentration, lifetime, and reactivity in different atmospheric layers are crucial in order to gain a better understanding of the complex mechanisms that lead to atmospheric or climatic changes and potential adverse health effects.[1]

Pollutants of particular interest are halogenated alkanes (CFCs, halons, HCFCs, HFCs, PFCs), mainly because of their central role in ozone layer depletion and global warming.[2−5] The monitoring of halogenated alkanes at or near ground level can be done routinely using a variety of sensitive and selective analysis techniques, often using on-site air sampling and off-line gas chromatography combined with mass spectrometry (GC/MS),[6] microwave-induced plasma atomic emission spectroscopy (GC/MIP-AES),[7,8] or flame ionization detection (GC/FID).[5] On-line, in situ approaches have also been proposed, using, for example, open-path spectroscopic techniques such as Fourier transform infrared spectroscopy (FT-IR) and tunable diode laser infrared spectroscopy (TDLAS) to provide the advantage of in situ measurements by propagating a light beam through the system to be monitored and using the absorption "fingerprint" of halogenated alkanes in the infrared region from 7 to 12.5 μm.[9−11]

The possibility to perform real-time, on-line monitoring of halocarbons has also been demonstrated using at least two laser-based techniques that do not rely on molecular absorption of IR light: laser-induced breakdown spectroscopy (LIBS) and laser photofragmentation/fragment detection (PF/FD). Typical limits of detection (LOD) for the analysis of halogenated alkanes by LIBS are in the low ppmw range with selectivity usually limited to classes of compounds.[12−15] PF/FD relies on the use of one or more lasers for photolysis of the analyte species and spectroscopic detection of the characteristic photofragments. Good analytical performance (ppm to ppb detection limits) as well as good selectivity for classes of compounds were generally obtained.[16,17]

Monitoring at higher altitude is somewhat more challenging. Measurement strategies usually involve either bringing the sample to the instrument, i.e., collecting samples and analyzing them afterward in the laboratory,[6] or bringing the instrument to the sample, for example, using balloon-borne instruments to look at

* To whom correspondence should be addressed. Phone: (418) 656-3287. Fax: (418) 656-7916. E-mail: denis.boudreau@chm.ulaval.ca.

[†] Department of Chemistry.

[‡] Department of Physics, Physical Engineering and Optics.

(1) Sigrist, M. W. In *Air Monitoring by Spectroscopic Techniques*; Sigrist, M. W., Ed.; Wiley: New York, 1994; pp 1−26.
(2) Molina, M. J.; Rowland, F. S. *Nature* **1974**, *249*, 810−812.
(3) Stemmler, K.; O'Doherty, S.; Buchmann, B.; Reimann, S. *Environ. Sci. Technol.* **2004**, *38*, 1998−2004.
(4) Dolin, E. J. *Light Met. Age* **1999**, *57*, 56−67.
(5) Rhoderick, G.; Chu, P.; Dolin, E.; Marks, J.; Howard, T.; Lytle, M.; McKenzie, L.; Altman, D. *Fresenius' J. Anal. Chem.* **2001**, *370*, 828−833.
(6) Mangani, G.; Berloni, A.; Maione, M. *J. Chromatogr., A* **2003**, *988*, 167−175.
(7) Koch, J.; Okruss, M.; Franzke, J.; Florek, S. V.; Niemax, K.; Becker-Ross, H. *Spectrochim. Acta, Part B* **2004**, *59*, 199−207.
(8) Abdillahi, M. M. *J. Chromatogr. Sci.* **1990**, *28*, 613−616.
(9) Chu, P. M. *Anal. Bioanal. Chem.* **2003**, *376*, 305−307.
(10) Hanst, P. L.; Hanst, S. T. In *Air Monitoring by Spectroscopic Techniques*; Sigrist, M. W., Ed.; Wiley: New York, 1994; pp 335−470.
(11) Gamble, H. A.; Mackay, G. I.; Karecki, D. R.; Pisano, J. T.; Schiff, H. I. *Light Met.* **2001**, 275−281.
(12) Haisch, C.; Niessner, R.; Matveev, O. I.; Panne, U.; Omenetto, N. *Fresenius' J. Anal. Chem.* **1996**, *356*, 21−26.
(13) Cremers, D. A.; Radziemski, L. J. *Anal. Chem.* **1983**, *55*, 1252−1256.
(14) Dudragne, L.; Adam, P. H.; Amouroux, J. *Appl. Spectrosc.* **1998**, *52*, 1321−1327.
(15) Williamson, C. K.; Daniel, R. G.; McNesby, K. L.; Miziolek, A. W. *Anal. Chem.* **1998**, *70*, 1186−1191.
(16) Sausa, R. C.; Simeonsson, J. B., U.S. Patent 5,866,073, 1999.
(17) Simeonsson, J. B.; Sausa, R. C. *TrAC, Trends Anal. Chem.* **1998**, *17*, 542−550.

10.1021/ac049425k CCC: $27.50
Published on Web 07/10/2004

IR absorption bands in the solar spectrum[10] or aircraft-based PF techniques.[17] While the latter strategy provides an unmatched richness of information, i.e., composition of the atmosphere with high sensitivity and dynamic range at a precise location in space and time, it cannot be easily used for routine analysis in a cost-effective manner. On the other hand, open-path techniques such as FT-IR and TDLAS, because they only provide path-averaged concentration values over line-of-sight measurements, cannot be used to obtain altitude-resolved halocarbon concentrations from the ground, while the relatively high laser fluences required by LIBS and PF/FD [i.e., the laser beam(s) are usually focused with short (i.e., < 1 m) focal length lenses] hinder their use for long-range remote sensing.

The light detection and ranging (LIDAR) technique is certainly one of the most effective and attractive tools for remote sensing of the atmosphere. It is based on the time-resolved detection of atmospheric backscatter signals emitted from laser pulses propagating into the atmosphere.[18] The probed path can easily be varied, and the signals provide range-resolved information, allowing the determination of 3-D distributions of atmospheric trace gases and aerosols over large areas. Different physical and chemical information can also be obtained from LIDAR backscatter signals along the probed path according to the physical phenomenon under study (i.e., optical absorption of the backscattered light, laser-induced fluorescence, Raman, Mie, and Rayleigh backscattering). Differential optical absorption spectroscopy (DOAS) can also be used in a LIDAR configuration (usually called DIAL for differential absorption LIDAR[19,20]). In that configuration, one wavelength is set to an absorption peak of the target molecule while a second wavelength is set off-peak. The difference measured in the backscattered signals is used to monitor the concentration of the target species along the propagation path. With such techniques, the ability to detect more than one pollutant—or even a single one, in the case of DIAL—generally relies on the use of several probing lasers, or on fast wavelength switching of a wide spectral range tunable laser such as liquid dye lasers and optical parametric oscillators. As pointed out by Kasparian et al.,[21] traditional LIDAR-based measurements basically require multiple light sources for what is essentially a single component experiment.

It has been shown recently that the use of high-power, ultrashort laser pulses (femtosecond, multi-terawatt) for LIDAR experiments allows the measurement of several target atmospheric species simultaneously.[21,22] Briefly, the propagation of intense femtosecond pulses in the atmosphere creates low-density plasma columns left behind by the continuous series of self-foci of the propagating laser pulse. These plasma columns, referred to as filaments,[23,24] are created by a dynamic interplay between two nonlinear effects, i.e., Kerr self-focusing in the neutral gas and subsequent defocusing by the plasma that is generated at the self-foci through multiphoton/tunnel ionization of the molecules and atoms.[22,25] The nonlinear propagation of the intense femtosecond pulses in air induces a spectral broadening of the initial pulse through the physical process of supercontinuum generation (SCG), often termed white-light laser generation.[22,26] For a pump wavelength centered at 800 nm, this supercontinuum has been shown to extend from 300 nm up to 4.5 μm.[27] The backward scattering of the white-light laser pulse combined with linear absorption spectroscopy has been used for atmospheric remote sensing of major constituents such as oxygen and water vapor, allowing the determination of relative humidity at a remote distance. Measurement of tropospheric ozone distribution in urban areas was also demonstrated at the $\mu g/m^3$ level.[21,28]

While this technique looks extremely promising, it implies, for constituents having either a low concentration or low absorption cross section, the integration of the absorption along an extended path, which affects the ability to make range-resolved measurements with high spatial resolution. Furthermore, LIDAR applications using the near-infrared side of the supercontinuum also remain a challenge.[29] While it is true that many important atmospheric species have their strongest absorption features in this spectral region, the intensity of the white-light supercontinuum drops exponentially in intensity as a function of wavelength, by more than 4 orders of magnitude from the pump wavelength (800 nm) up to 2.5 μm, and by another order of magnitude from 2.5 to 4.5 μm.[27] Recently, the detection of LIDAR signals in the NIR region up to 1.7 μm using the supercontinuum emitted from light filaments propagating in the atmosphere was reported,[29] although the application of this technique to the actual detection of trace molecules in this spectral region has not yet been reported.

In this work, we report on the study of another phenomenon related to the propagation of ultrafast and intense laser pulses in air[30] for the in situ determination of halogenated alkanes in the atmosphere. It was shown previously that the peak intensity inside a filament is limited to about 5×10^{13} W/cm^2 in air due to the competition between self-focusing and defocusing[31−33] and that this intensity can be reached at a remote distance from the source.[21] At these high intensities, most molecules undergo multiphoton/tunnel ionization (MPI) and fragmentation. Many of the ionization and fragmentation products are excited and emit

(18) Sigrist, M. W. *Air Monitoring by Spectroscopic Techniques*; Wiley: New York, 1994.
(19) Panne, U. *TrAC, Trends Anal. Chem.* **1998**, *17*, 491−500.
(20) Svanberg, S. In *Air Monitoring by Spectroscopic Techniques*; Sigrist, M. W., Ed.; Wiley: New York, 1994; pp 85−161.
(21) Kasparian, J.; Rodriguez, M.; Mejean, G.; Yu, J.; Salmon, E.; Wille, H.; Bourayou, R.; Frey, S.; Andre, Y. B.; Mysyrowicz, A.; Sauerbrey, R.; Wolf, J. P.; Woste, L. *Science* **2003**, *301*, 61−64.
(22) Kandidov, V. P.; Kosareva, O. G.; Golubtsov, I. S.; Liu, W.; Becker, A.; Akozbek, N.; Bowden, C. M.; Chin, S. L. *Appl. Phys. B* **2003**, *77*, 149−165.
(23) Brodeur, A.; Chien, C. Y.; Ilkov, F. A.; Chin, S. L.; Kosareva, O. G.; Kandidov, V. P. *Opt. Lett.* **1997**, *22*, 304−306.
(24) Lange, H. R.; Grillon, G.; Ripoche, J.-F.; Franco, M. A.; Lamouroux, B.; Prade, B. S.; Mysyrowicz, A.; Nibbering, E. T. J.; Chiron, A. *Opt. Lett.* **1998**, *23*, 120−122.
(25) Couairon, A. *Appl. Phys. B* **2003**, *76*, 789−792.
(26) Chin, S. L.; Brodeur, A.; Petit, S.; Kosareva, O. G.; Kandidov, V. P. *J. Nonlinear Opt. Phys. Mater.* **1999**, *8*, 121−146.
(27) Kasparian, J.; Sauerbrey, R.; Mondelain, D.; Niedermeier, S.; Yu, J.; Wolf, J. P.; Andre, Y. B.; Franco, M.; Prade, B.; Tzortzakis, S.; Mysyrowicz, A.; Rodriguez, M.; Wille, H.; Woste, L. *Opt. Lett.* **2000**, *25*, 1397−1399.
(28) Rairoux, P.; Schillinger, H.; Niedermeier, S.; Rodriguez, M.; Ronneberger, F.; Sauerbrey, R.; Stein, B.; Waite, D.; Wedekind, C.; Wille, H.; Woste, L.; Ziener, C. *Appl. Phys. B* **2000**, *71*, 573−580.
(29) Mejean, G.; Kasparian, J.; Salmon, E.; Yu, J.; Wolf, J. P.; Bourayou, R.; Sauerbrey, R.; Rodriguez, M.; Woeste, L.; Lehmann, H.; Stecklum, B.; Laux, U.; Eisloeffel, J.; Scholz, A.; Hatzes, A. P. *Appl. Phys. B* **2003**, *77*, 357−359.
(30) Luo, Q.; Liu, W.; Chin, S. L. *Appl. Phys. B* **2003**, *76*, 337−340.
(31) Kasparian, J.; Sauerbrey, R.; Chin, S. L. *Appl. Phys. B* **2000**, *71*, 877−879.
(32) Becker, A.; Akozbek, N.; Vijayalakshmi, K.; Oral, E.; Bowden, C. M.; Chin, S. L. *Appl. Phys. B* **2001**, *73*, 287−290.
(33) Lange, H. R.; Chiron, A.; Ripoche, J. F.; Mysyrowicz, A.; Breger, P.; Agostini, P. *Phys. Rev. Lett.* **1998**, *81*, 1611−1613.

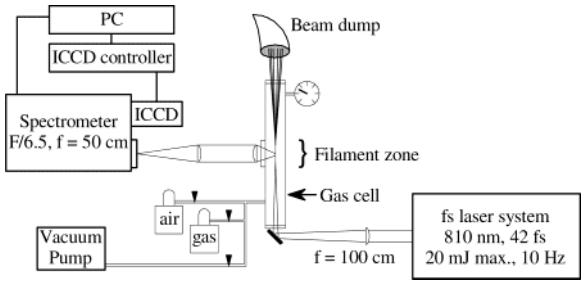

Figure 1. Experimental setup used for femtosecond laser-induced fluorescence.

characteristic fluorescence. In air, the so-called "clean fluorescence" of nitrogen molecules and ions is routinely observed from the filaments.[34,35] Due to the low plasma electron density inside the filament ($n_e \approx 10^{14}-10^{16}$ in air vs $10^{16}-10^{18}$ for nanosecond laser-induced plasmas[36]), continuum emission from the plasma is quite low and does not mask the spectral features compared to what is usually observed from the optical breakdown induced by longer pulses.[34,35] Recent experiments have shown that clean nitrogen fluorescence, free from white-light supercontinuum, can be detected in the backward direction.[37] It was also shown recently that the backscattered fluorescence from nitrogen molecules in a filament generated by a femtosecond Ti:sapphire laser pulse in air can be amplified (ASE).[30] This makes femtosecond-induced clean fluorescence very promising for the remote sensing of atmospheric constituents. In this work, we demonstrate that clean and characteristic fragment fluorescence can be obtained inside a filament for fluorine-containing halocarbons, notably PFCs CF_4 and C_2F_6. This would allow the remote sensing of such pollutants in the vicinity of point sources such as aluminum production plants as well as the evaluation of their distribution in the atmosphere.

EXPERIMENTAL SECTION

Laser System. A detailed description of the high-power femtosecond laser system used for this work has been given elsewhere,[37] and only a brief overview will be given herein. The system consists of a Ti:sapphire oscillator followed by a regenerative amplifier, a two-pass Ti:sapphire amplifier, and a pulse compressor (Spectra Physics). The pulse duration at the output of the compressor is typically 42 fs, and the central wavelength is 810 nm with a bandwidth of 23 nm (fwhm). The maximum output energy of the system is about 20 mJ per pulse at a repetition rate of 10 Hz.

Femtosecond Laser-Induced Fluorescence Setup. The laser beam is focused by a single plano-convex lens (100-cm focal length) into a cylindrical stainless steel gas cell (4-cm i.d. × 135-cm length) containing the gaseous species under study (see Figure 1). The laser focusing optics and windows are made of CaF_2 and antireflection coated at 800 nm. A mechanical vacuum pump and precision vacuum valves are used to control the composition of the halocarbon/air mixtures introduced into the gas cell. Different halocarbon concentrations were obtained by diluting halocarbons with high-purity air, with partial gas pressures being monitored by differential capacitance manometers (Baratron). Due to the restrictions imposed on the use of HCFCs in Canada, HCFC-124 (2-chloro-1,1,1,2-tetrafluoroethane, Dupont) was purchased as a refrigerant from a local dealer, and the purity is therefore unknown. CF_4 and C_2F_6 were obtained as mixtures in air (25 ± 2% v/v, Praxair Canada). All the experiments for the current study were carried out at atmospheric pressure.

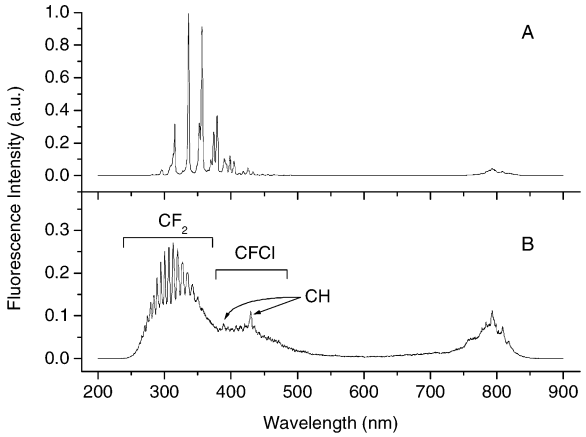

Figure 2. Spectra obtained for femtosecond laser-induced fluorescence: (A) air; (B) HCFC-124. Laser pulse energy = 5 mJ, detector gate delay set to 0 ns with respect to the pump laser, 25 ns gate width, 60 laser shots accumulated. Note the different intensity scales used for each spectrum.

The laser pulse energy used in the experiments was typically 5 mJ, which creates a filament inside the gas cell with a length of ca. 10 cm. The fluorescence emission from the filament was collected at 90° to the laser propagation axis through a fused-silica window and the central, most intense part of the filament was imaged by two plano-convex lenses (fused silica, focal lengths of 11 and 25 cm) parallel and onto the entrance slit of a spectrometer (Acton Research Corp., SpectraPro-500i SP-558, F/6.5, focal length 50 cm). The spectrometer was operated with either a 300 lines/mm grating for wide simultaneous spectral coverage or a 1200 lines/mm grating for higher spectral resolution. With a 10-μm entrance slit width, the nominal spectral resolution of the spectrometer is 0.05 nm for the 1200 lines/mm and 0.2 nm for the 300 lines/mm. The fluorescence was detected by an intensified CCD camera (Princeton Instruments, PI-MAX 512) featuring 512 × 512 pixels, a dynamic range of 16 bits, a maximum intensifier gain of 10^4, and a spectral range of 200−900 nm. This gated multichannel detector (minimum gate width of 2 ns) was instrumental in the optimization of background signal rejection and signal-to-noise ratios, while enabling the probing of nanosecond-scale spectroscopic dynamic processes.

RESULTS AND DISCUSSION

Figure 2A shows the time-resolved, clean UV−vis fluorescence spectrum obtained for pure air (halocarbon free) in the gas cell. The bands observed in the 300−400 nm region were previously assigned to the first negative band ($B^2\Sigma_u^+ \rightarrow X\ ^2\Sigma_g^+$) of N_2^+ and the second positive band ($C^3\Pi_u \rightarrow B^3\Pi_g$) of N_2.[34,35] It has been demonstrated that nitrogen molecules are ionized and excited inside the filament through the ejection of an inner valence

(34) Talebpour, A.; Abdel-Fattah, M.; Chin, S. L. *Opt. Commun.* **2000**, *183*, 479−484.
(35) Talebpour, A.; Abdel-Fattah, M.; Bandrauk, A. D.; Chin, S. L. *Laser Phys.* **2001**, *11*, 68−76.
(36) Simeonsson, J. B.; Miziolek, A. W. *Appl. Opt.* **1993**, *32*, 939−947.
(37) Luo, Q.; Hosseini, S. A.; Ferland, B.; Chin, S. L. *Opt. Commun.* **2004**, *233*, 411−416.

electron,[38,39] radiative relaxation from these excited states giving rise to nitrogen ion fluorescence. Electron−ion recombination then leads to the emission of the second positive band of the neutral N_2 molecule. In the current experiment, the integration time ("ICCD gate width") was set to 25 ns with 0 ns delay ("ICCD gate delay") with respect to the femtosecond laser pump pulse. Previous reports showed that the fluorescence lifetime of the nitrogen molecules (N_2/N_2^+) was ≤2ns.[37,40] Thus, the 25-ns integration time used was largely sufficient to collect all the fluorescence emitted from the filament.

Rayleigh scattering at the pump laser wavelength can be observed around 800 nm, with some broadening of the pump pulse. Notably, neither atomic emission lines nor strong continuum emission appear in the spectrum, which is consistent with previous observations.[34,35] The spectrum in Figure 2 is representative of "pure" filamentation, as opposed to the breakdown (see ref 41) created at the geometrical focus using longer (picosecond to nanosecond) pulse durations, the emission spectrum of which consists of a continuum superimposed with neutral and ionic atomic lines.[34,35]

Figure 2B shows the UV−vis fluorescence spectrum obtained with pure HCFC-124 inside the gas cell. HCFC-124 was used for this study because it was the only pure halocarbon available for this experiment. The band centered around 300 nm can be attributed to emission from the excited difluorocarbene radical (CF_2) molecular fragment. Due to its importance in atmospheric chemistry and ion plasma etching, CF_2 has been the subject of many spectroscopic and kinetic studies.[42−45] On the basis of previous observations, this emission band is attributed to the $A^1B_1 \rightarrow X^1A_1$ transition. The vibrational structure is clearly visible in the spectrum, despite the low resolution offered by the 300 lines/mm grating.

CF_2 has been observed as a stable product in many laser photofragmentation experiments involving diverse fluorinated alkanes.[42−45] It is also known to be a direct product resulting from the stratospheric photolysis of PFCs, CFCs, and HCFCs.[45] These photochemical pathways result from the relatively high strength of the C−F bond (typically 485 kJ/mol as compared to, e.g., 350 kJ/mol for the C−C bond). Fragmentation of the parent molecule (or parent ion)[46] and of heavier fragments is certainly driven by weaker bonds, which leads in the end to the production of the stable radical CF_2.

The spectral region around 430 nm contains the spectral signature of different molecular fragments. The narrow band around 430 nm emerging on top of a much broader structure is attributed to the CH radical ($A^2\Delta \rightarrow X^2\Pi$). The CH $B^2\Sigma \rightarrow X^2\Pi$ transition around 389 nm is overshadowed by what could be the CFCl emission ($A \rightarrow X$), as observed by Rossberg et al. in the 350−450 nm region.[46] It should be noted again that neither atomic emission lines nor continuum emission are observed in the spectrum (i.e., the strongest expected lines are C I at 247.86 nm, F I at 685.60 nm, Cl I at 837.59 nm, H I_α at 656.20 nm). This is in contrast with typical results obtained from LIBS, where continuum emission followed by atomic emission dominates the spectrum.[12−15]

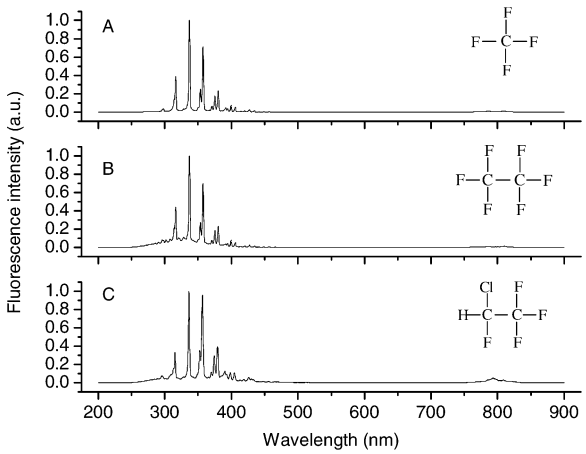

Figure 3. Femtosecond laser-induced fluorescence spectra for halocarbon/air mixtures. Concentration = 25% v/v for each mixture, laser pulse energy = 5 mJ, 0 ns gate delay with respect to pump pulse. (A) CF_4, 15 ns gate width, 200 accumulations. (B) C_2F_6, 15 ns gate width, 200 accumulations. (C) HCFC-124, 25 ns gate width, 60 accumulations.

Since CF_2 can be readily generated from many CF_2-containing halocarbons,[42] generation and detection of this spectral signature by femtosecond-induced filamentation represents a promising avenue for the remote sensing of such species in the atmosphere. However, in air and at low concentrations, the strong nitrogen emission interferes with CF_2 emission, preventing the detection of the targeted species, as shown in Figure 3. The characteristic CF_2 emission band can hardly be observed for 25% mixtures of halocarbons in air at atmospheric pressure for these experimental conditions. It is even more dramatic for CF_4, where the spectrum seems almost free from any CF_2 fluorescence. It should be noted, however, that spectral features specific to HCFC-124 (CH and CFCl bands) can be observed amidst the N_2/N_2^+ spectral background in the 400 nm region (Figure 3C). Another observation of importance is that we have not observed in these experiments any emission from electronically excited OH, which is known to have a strong band around 308 nm[1] that could interfere with CF_2 fluorescence.

The key to overcoming interference from atmospheric nitrogen lies in the different fluorescence lifetimes of CF_2 and N_2/N_2^+, as shown by the time-resolved fluorescence spectra obtained for a mixture of 25% C_2F_6 in air (Figure 4). These spectra were acquired with a fixed detector gate width of 5 ns and varying delay time (τ) with respect to the pump pulse, starting from $\tau = -5$ ns (before the pump pulse) up to $\tau = 110$ ns. Each spectrum shows the time-resolved fluorescence signal averaged over 200 laser pulses. When the filament is initiated ($\tau = 0$ ns), one can observe a spectrum that is characteristic of N_2/N_2^+ emission while CF_2 emission cannot yet be observed. The spectrum taken at $\tau = 5$ ns contains

(38) Talebpour, A.; Bandrauk, A. D.; Yang, J.; Chin, S. L. *Chem. Phys. Lett.* **1999**, *313*, 789−794.
(39) Becker, A.; Bandrauk, A. D.; Chin, S. L. *Chem. Phys. Lett.* **2001**, *343*, 345−350.
(40) Martin, F.; Mawassi, R.; Vidal, F.; Gallimberti, I.; Comtois, D.; Pepin, H.; Kieffer, J. C.; Mercure, H. P. *Appl. Spectrosc.* **2002**, *56*, 1444−1452.
(41) Liu, W.; Luo, Q.; Chin, S. L. *Chin. Opt. Lett.* **2003**, *1*, 56−59.
(42) King, D. S.; Schenck, P. K.; Stephenson, J. C. *J. Mol. Spectrosc.* **1979**, *78*, 1−15.
(43) Vetter, R.; Reuter, W.; Peyerimhoff, S. D. *Chem. Phys.* **1992**, *161*, 379−392.
(44) Chau, F.-t.; Dyke, J. M.; Lee, E. P.-f.; Wang, D.-c. *J. Electron Spectrosc. Relat. Phenom.* **1998**, *97*, 33−47.
(45) Cameron, M. R.; Kable, S. H.; Bacskay, G. B. *J. Chem. Phys.* **1995**, *103*, 4476−4483.
(46) Rossberg, M.; Wolbrandt, J.; Strube, W.; Linke, E. *J. Mol. Struct.* **1995**, *348*, 421−424.

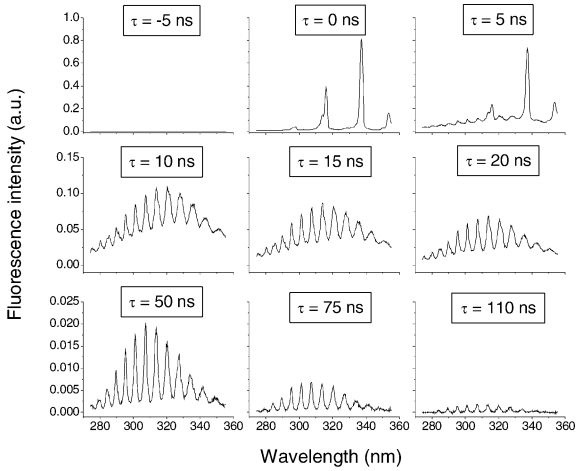

Figure 4. Time-resolved fluorescence spectra obtained for a mixture of 25% C_2F_6 in air. Laser pulse energy = 5 mJ. For each delay with respect to the pump pulse (τ), 200 shots were averaged. ICCD gate width = 5 ns for all measurements. Note the different intensity scales used for each row of spectra.

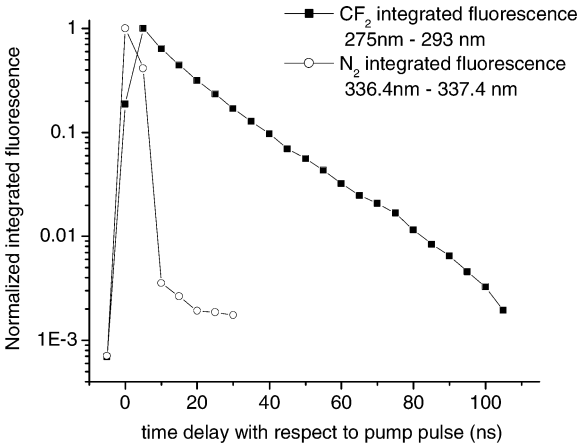

Figure 5. Fluorescence decay curves for CF_2 and N_2. Laser pulse energy = 5 mJ, 5 ns gate width, 200 laser shots accumulated.

emission from both species, while all subsequent spectra show clear CF_2 fluorescence emission without any trace of N_2/N_2^+ emission.

Figure 5 shows the normalized fluorescence decay curves obtained for the CF_2 fragment and N_2 by integrating a selected wavelength interval on a time-resolved spectrum (the integration wavelength range is specified on the figure). For N_2, the time-resolved spectrum was acquired using pure air in the gas cell to avoid any CF_2 contribution, while we used a 25% C_2F_6 in air mixture for the CF_2 lifetime measurements, in order to include any collisional quenching effect induced by air (N_2) on the fluorescence lifetime of CF_2. In this case, the integration interval was set around 285 nm, off the maximum of the CF_2 emission but in a spectral region free from any N_2 fluorescence. One can observe that the N_2 fluorescence lifetime is much shorter than that of CF_2 and that the peak fluorescence intensity of CF_2 is delayed with respect to the pump pulse, whereas N_2 reaches maximum fluorescence intensity in the first gate interval (which includes the pump pulse). This certainly suggests that different mechanisms may be responsible for the production of excited CF_2 versus that of excited N_2 species, e.g., ionization and fragmentation of the parent molecule into a precursor fragment that could lead,

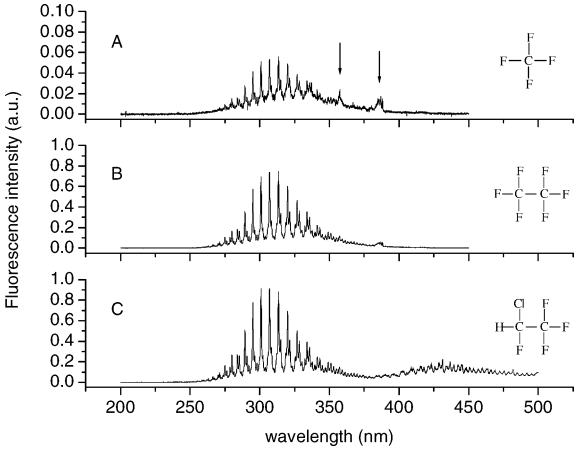

Figure 6. Time-gated fluorescence spectra for 25% halocarbon/air mixtures. Gate delay with respect to pump laser pulse = 10 ns, gate width = 105 ns, 200 accumulations, laser pulse energy = 5 mJ. Note the different intensity scales used for spectrum A (vs B and C).

upon collisions, to the production of excited CF_2. Electron capture by the parent molecule followed by dissociation could also be a plausible path for the production of excited CF_2. These studies are underway but are beyond the scope of the present paper.

As shown in Figure 6, the longer fluorescence decay observed for the CF_2 fragment allows the measurement of a clean CF_2 spectrum, free from N_2 emission bands, by properly adjusting the time delay with respect to the femtosecond pump pulse as well as the integration period (gate width). One can also observe in Figure 6C that the CFCl band ($A \rightarrow X$) around 430 nm is also free from N_2 interference. For this experiment, the experimental parameters were the same as those in Figure 3, except for gate width and delay. In the present case, the acquisition was started 10 ns after the pump laser pulse and lasted for 105 ns. The spectra obtained in this manner are free from nitrogen fluorescence, with the exception of small features around 360 and 385 nm (as shown in Figure 5, a weak tail from nitrogen fluorescence persists 10 ns after the onset of the pump pulse). A finer adjustment of the gate delay would presumably have eliminated this contribution to the background signal.

It can also be observed from Figure 6 that the CF_2 spectrum obtained from CF_4 shows a much weaker fluorescence yield as compared to that obtained from C_2F_6 or HCFC-124 with the present experimental conditions. These results clearly show the role of molecular structure on the extent of the ionization and fragmentation mechanisms leading to the production of excited CF_2. In cases where the overall CF_2-containing halocarbon concentration needed to be determined quantitatively from a mixture of different species, differing sensitivities would require the selective measurement of individual species, for example, using the fluorescence of other species-specific fragments such as CFCl. Finally, the CF_2 fluorescence spectra show that the population of the vibrational levels is very similar regardless of the parent molecule studied (CF_4, C_2H_6, or C_2HClF_4). This could be the indication of a common precursor or common mechanism resulting in the production of excited CF_2. Preliminary TOFMS experiments conducted with these molecules suggest that CF_3, one of the most prevalent fragment ions observed, could be this common precursor fragment.

This temporal background signal discrimination could easily be implemented for the detection of halocarbons by femtosecond laser-induced fluorescence in a LIDAR configuration (i.e., backward signal detection, as opposed to the side-detection configuration used in the present study). The length and distance of the filament could be determined from the short-lived N_2 fluorescence signal[37] and, using this information to set and adequate gate delay, one could temporally separate fluorescence signals from N_2 and CF_2. This would potentially be applicable to the measurement of other molecular fragments having fluorescence lifetimes longer than that of N_2.

It should be pointed out that the effective use of the time-resolved strategy in a backward detection scheme is only valid if the filament giving rise to the fluorescence emission possesses a localized high intensity at one point along the propagation axis (as opposed to a long, uniform plasma column). For midrange propagation experiments in air (over 100 m), it has been recently reported that the strongest part of the N_2 emission inside a filament comes from the earliest self-focusing region.[47] When pulse parameters are well controlled to induce the formation of a single filament, strong N_2 fluorescence is observable only for a few meters from the earliest self-focusing region. By optimizing parameters such as pulse chirping, beam size,[48,49] and divergence, it is also possible to control the onset of filamentation and to force the generation of a strong, short filament.

Analytical figures of merit were evaluated for C_2F_6 in air at atmospheric pressure using the time-resolved acquisition strategy discussed above. In order to improve light collection efficiency, the experimental setup was slightly modified. First, the ICCD camera was removed from the spectrometer and used in combination with a band-pass filter (UG11, Corion/Spectra-Physics) to integrate light emission over all CF_2 lines between 260 and 385 nm. In addition, since the filament could not be imaged entirely onto the ICCD detector by the optical arrangement used during the filament characterization studies, a shorter filament was produced by the combination of a shorter focal length (50 cm) focusing lens, a lower pulse energy (500 μJ) and a shorter gas cell (5-cm i.d. $\times$ 40-cm long, same window materials and dimensions). In this manner, the entire filament length (approximately 3 cm) could be imaged onto the detector with a pair of plano-convex lenses (fused silica, 6.7- and 11-cm focal length). The fluorescence signal was taken as the integration of the entire acquired image. Different concentrations of C_2F_6 in air (ranging from 15% to 0.05%) were prepared starting from the more concentrated mixture available (25%) and subsequently decreasing the pressure inside the gas cell and backfilling to atmospheric pressure with pure air. The background signal and associated noise were recorded in a similar fashion with pure air inside the gas cell. Using a gate width of 70 ns and a gate delay of 10 ns with respect to the pump pulse, we obtained a 3σ detection limit of 500 ppmv. The calibration curve is linear over the concentration range studied, and the dynamic range extends over at least 3 orders of magnitude (Figure 7). We found that the LOD attainable with this instrumental configuration is limited by the background fluctuations from the remaining N_2 fluorescence signal in the spectral region of interest. Therefore, increasing the light collection efficiency using the filter-based optical arrangement did not significantly improve the analytical figures of merit. An instrumental detection limit of 8 ppmv, comparable to LIBS detection limits for similar compounds, was calculated by measuring the background noise at the current detection sensitivity without firing the pump laser. Arguably, other molecular fragments having fluorescence intensity comparable to that of CF_2 but longer fluorescence lifetimes or different emission spectral range could provide similar detection limits.

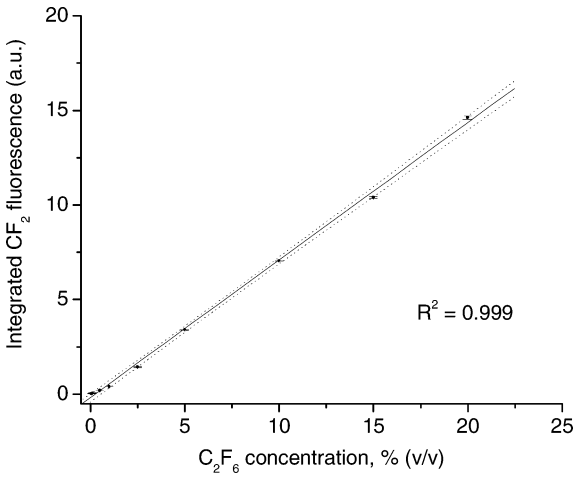

Figure 7. Calibration curve obtained for the detection of C_2F_6 in air using femtosecond laser-induced fluorescence of the CF_2 fragment.

The detection limit achieved in this preliminary study is modest and does not yet match the sensitivity required to measure pollutants at the trace level. However, there are many possible means to improve both sensitivity and selectivity and therefore make this technique into a viable approach for the remote sensing of pollutants with a single laser source. For example, detection of the fluorescence signal in the backward direction could provide a selective enhancement of the CF_2 fragment fluorescence versus that of N_2, resulting from signal amplification through amplified spontaneous emission (ASE) along the laser propagation axis (which has already been demonstrated for N_2 in air[30]). Since CF_2 has a significantly longer lifetime, it could therefore be amplified over a longer path, giving rise to a selective signal enhancement versus N_2. Testing this hypothesis will require the use of a gas cell at least a few meters in length, which has not yet been done in the laboratory due to space limitations.

Another approach involves the use of adaptively shaped ultrafast laser pulses, as recently suggested by Méjean et al.[48] Briefly, the control of the relative spectral phase and intensity of the femtosecond pulse enables the selective control of physical processes such as ionization, fragmentation, and excitation, as shown recently in remarkable experiments by Levis at al.[50] for the selective control of molecular fragmentation and by Brixner et al.[51] for chemically selective molecular excitation. Such an

(47) Hosseini, S. A.; Luo, Q.; Ferland, B.; Liu, W.; Akoezbek, N.; Roy, G.; Chin, S. L. *Appl. Phys. B* **2003**, *77*, 697−702.
(48) Mejean, G.; Kasparian, J.; Yu, J.; Frey, S.; Salmon, E.; Wolf, J. P. *Appl. Phys. B* **2004**, *78*, 535−537.
(49) Wille, H.; Rodriguez, M.; Kasparian, J.; Mondelain, D.; Yu, J.; Mysyrowicz, A.; Sauerbrey, R.; Wolf, J. P.; Woste, L. *Eur. Phys. J.: Appl. Phys.* **2002**, *20*, 183−190.
(50) Levis, R. J.; Menkir, G. M.; Rabitz, H. *Science* **2001**, *292*, 709−713.
(51) Brixner, T.; Damrauer, N. H.; Niklaus, P.; Gerber, G. *Nature* **2001**, *414*, 57−60.

approach could result in an enhancement of the CF_2/N_2 fluorescence ratio and improved LODs, as well as the possibility to selectively measure individual species such as CF_4, C_2F_6, and C_2HClF_4, which would allow in turn the ability to correct for differing detection sensitivities and facilitate the quantitative determination of the overall halocarbon concentration in air.

Finally, another interesting approach could combine the potential advantages offered by the present femtosecond laser-induced fluorescence technique and the white-light absorption approach in a pump−probe experiment scheme. For example, one could generate molecular fragments at a precise remote location by generating a strong single filament with the first pulse and probe these fragments in the UV−vis using white-light absorption generated by the delayed second pulse. This would overcome problems associated with the low spectral intensity of the supercontinuum in the IR and the presence of H_2O/CO_2 absorption bands while avoiding any detrimental spectral interference problem related to N_2 emission.

CONCLUSION

We have presented herein a novel fluorescence detection approach applicable to the remote sensing of atmospheric pollutants using intense femtosecond laser pulses. Fragment fluorescence in the UV−vis could become a complementary technique to the white-light approach based on absorption, especially for molecules that mostly absorb in the mid-IR, where major atmospheric constituents such as water vapor or carbon dioxide limit atmospheric transmission and degrade detection sensitivity as well as selectivity.

We have shown that, due to different fluorescence lifetimes, time-resolved detection of CF_2 fluorescence emission allows one to overcome a spectral interference arising from N_2 fluorescence, at the expense of a reduction in CF_2 fluorescence detection sensitivity but with a substantial gain in signal-to-background ratio. With the current experimental setup, we have calculated a 3σ detection limit of 500 ppmv for C_2F_6 in air, which is limited by the remaining background N_2 emission. An instrumental detection limit of 8 ppmv has been calculated with the current calibration sensitivity.

To make this technique into a viable approach for remote sensing of pollutants at the trace level with a single laser source, both sensitivity and selectivity will have to be improved in order to achieve better detections limits. Possible improvements might be obtained from signal amplification through amplified spontaneous emission (ASE) along the laser propagation axis, as well as from the use of adaptively shaped ultrafast laser pulses to selectively enhance the fluorescence signal of the target species.

ACKNOWLEDGMENT

The authors acknowledge the Natural Sciences and Engineering Research Council of Canada (NSERC), Fonds Québécois de Recherche sur la Nature et les Technologies (FQRNT), Canada Research Chair, Canada Foundation for Innovation (CFI), Valorisation-Recherche Québec−Femtotech, Canadian Institute of Photonics Innovation (CIPI), and Defense Research and Development Canada (DRDC) for their financial support.

Received for review April 16, 2004. Accepted June 9, 2004.

AC049425K